Front. Phys. 11(3), 118501 (2016)
DOI 10.1007/s11467-015-0528-3

RESEARCH ARTICLE

Optical properties of Au-core Pt-shell nanorods studied using FDTD simulations

Jian-Bo Liu[1,*], Lin Long[2], Yu-Shi Zhang[1], Yue-Ping Wang[1], Feng-Shou Liu[1], Wei-Yao Xu[1], Ming-Ji Zong[1], Lei Ma[1], Wen-Qi Liu[3], Hui Zhang[3], Jiao Yan[3], Jia-Qi Chen[3], Ying-Lu Ji[3], Xiao-Chun Wu[3,†]

[1] *College of Opto-electronic Engineering, Zaozhuang University, Zaozhuang 277100, China*

[2] *Zaozhuang Municipal Center for Disease Control and Prevention, Zaozhuang 277100, China*

[3] *CAS Key Laboratory of Standardization and Measurement for Nanotechnology, National Center for Nanoscience and Technology, Beijing 100190, China*

*Corresponding authors. E-mail: *linyibm@163.com, †wuxc@nanoctr.cn*

Received August 16, 2015; accepted October 10, 2015

Au-core/Pt-shell nanorods (Au@Pt NRs) have been prepared by a Au nanorod-mediated growth method, and they exhibit high electromagnetic field enhancements under coupling conditions. Boosted by a long-range effect of the high electromagnetic field generated by the Au core, the electromagnetic field enhancement can be controlled by changing the morphology of the nanostructures. In this study, we report the results on the simulations of the electromagnetic field enhancement using a finite difference time domain (FDTD) method, taking the real shapes of the Au@Pt NRs into account. Due to the "hot spot" effect, the electromagnetic field can be localized between the Pt nanodots. The electromagnetic field enhancement is found to be rather independent of the Pt content, whereas the local roughness and small sharp features might significantly modify the near-field. As the electromagnetic field enhancement can be tuned by the distribution of Pt nanodots over the Au-core, Au@Pt NRs can find potential applications in related areas.

Keywords gold, platinum, core-shell, nanorod, FDTD

PACS numbers 85.85.+j, 78.67.-n, 78.20.Bh

1 Introduction

Metal nanoparticles have been widely studied owing to their fundamental interests and practical applications. The optical properties of metal nanoparticles strongly depend on the size, shape, and environment of the particles [1–5]. On irradiation of lights with a specific wavelength, the surface plasmons in the metal particles can be excited, leading to an enhancement of the local electromagnetic field close to the particles [6–10]. Electromagnetic field enhancement is, in part, the basis behind surface-enhanced Raman scattering (SERS), a spectroscopic phenomenon discovered over 40 years ago and still perplexing to the scientific community in terms of its scientific origins and potential applications [11–15].

Various morphologies of metal nanostructures including nanorods [16], bowtie nanoantennas [17], nanoburgers [18], triangular nanoprisms [19], and nanopins [20] have been suggested for inducing the local enhancement of the electromagnetic field, and these nanostructures were further proved useful as SERS platforms [21]. Furthermore, the lightning rod effect (due to geometric factors) is considered to play a significant role in the electromagnetic field enhancement in the case of rod-shaped nanoparticles [22–24]. Currently only three "coinage metals" (Au, Ag, and Cu) are reported to provide the significant enhancements required, and this severely limits the breadth of practical applications [25, 26]. Although transition metals have much wider applications in electrodes and catalysts in electrochemistry and surface science, they are commonly considered as non-SERS-active substrates. SERS studies on colloidal Pt and roughened Pt surfaces have shown considerably smaller enhancement effects of Pt as compared to Au, Ag, and Cu [27]. In order to explore the potential applications and to optimize the SERS activity of the transition metal-based nanoparticles, Tian et al. have recently studied a strategy of "borrowing" high SERS activity from the Au-core [28, 29]. This approach makes use of the long-range effect of the high electromagnetic field created by the Au nanoparticles. Moreover, by forming

a core/shell structure with the Au nanorods, the surface plasmon resonance (SPR) band of the Pt nanostructures can be shifted from the ultraviolet region to visible and near-infrared regions, and this opens up the potential of using Pt nanostructures for SPR-based sensing.

In this paper, we report the design, characterization, and the electromagnetic field enhancement effects of the Au-core/Pt-shell nanorods (Au@Pt NRs). We have analyzed the SPR spectra and the near-field enhancement of the individual Au@Pt NRs of different growth modes using a finite difference time domain (FDTD) method. The widely used FDTD method in nanoplasmonic simulations provides a powerful numerical tool in studying the mechanism of the electromagnetic field enhancement and helps in the design of nanostructured systems [30].

2 Experiments

2.1 Chemicals and reagents

Sodium borohydride ($NaBH_4$), chloroauric acid ($HAuCl_4{\cdot}3H_2O$), cetyltrimethylammonium bromide (CTAB), potassium tetrachloroplatinate (II) (K_2PtCl_4), and silver nitrate ($AgNO_3$) were purchased from Alfa Aesar. Other chemicals used in the study were of at least analytical reagent grade and were purchased from Beijing Chemical Reagent Company (Beijing, China). Milli-Q water (18 MΩ·cm) was used as a solvent in all experiments.

2.2 Synthesis of Au@Pt NRs

Synthesis of Au nanorods (Au NRs): Au NRs were synthesized using a seed-mediated growth procedure, which is reported in the literature [31]. Initially, CTAB-capped Au seeds were synthesized via a chemical reduction of $HAuCl_4$ by $NaBH_4$. In a typical synthesis, CTAB (7.5 mL, 0.1 M) was mixed with $HAuCl_4$ (100 μL, 24 mM) and then diluted with water to form a 9.4 mL mixture, which was stirred using a magnetic stirrer. Ice-cold $NaBH_4$ (0.6 mL, 0.01 M) was then added to this solution, and the color of the mixture immediately turned from bright yellow to brown, indicating the formation of Au seeds. The Au seeds were used within 2–5 h of their preparation. To initiate the growth of Au nanorods, 120 μL of the Au seed solution was added to a growth solution containing CTAB (100 mL, 0.1 M), $HAuCl_4$ (2.04 mL, 24 mM), $AgNO_3$ (1.05 mL, 10 mM), and ascorbic acid (AA) (552 μL, 0.1 M). After 12 h, AA (55.2 μL, 0.1 M) was added two times to the mixture in 40 min intervals under stirring. The reaction was allowed to proceed for 24 h, and the Au NRs formed were purified by centrifugation at 12000 rpm for 5 min in two cycles. The precipitate was collected and redispersed in deionized water to form a 50 mL Au NR solution.

Synthesis of Au@Pt NRs: 1 mL of the Au NR solution was mixed with 12.5, 25, 42.5, and 250 μL of 2 mM $PtCl_4^{2-}$ aqueous solutions to obtain Pt/Au ratios of 0.05, 0.1, 0.17, 0.5, and 1, respectively. Then, 15 μL of 0.1 M AA was added and the volume of the resulting solution was made to 2 mL by dilution. The mixture was shaken vigorously and was placed in a water bath at 30 °C for 30 min. Within several minutes, the color of the solution was changed from pink-red to dark gray, suggesting the formation of Pt shells. 1 mL of 0.1 M CTAB was then added.

2.3 Characterization

The UV-Vis-NIR absorption spectra of the samples were recorded using Varian Cary 50. Scanning electron microscopy (SEM) images were recorded and energy dispersive X-ray (EDX) analysis was carried out using a field emission scanning electron microscope (FESEM, Hitachi S-4800). Transmission electron microscopy (TEM) images were captured on a FEI TECNAI G2 F20 U-TWIN at an accelerating voltage of 200 kV. 3 μL of the nanorod solution was dried on carbon-coated copper grids for 30 min, and TEM micrographs were recorded at a minimum of eight different regions in the grid. For size measurements, ca. 200 nanorods were considered.

2.4 FDTD calculations

FDTD calculations were performed with FDTD Solutions 8.11, developed by Lumerical Solutions, Inc. The absorption spectra and the electromagnetic field intensity enhancement contours were obtained from FDTD calculations on the Au@Pt NRs with Pt nanodots of different morphologies. The Pt nanodots were assumed to be spheres with a 3-nm diameter that are distributed uniformly on the Au nanorod surface. The length and width of the Au NRs were fixed at 54 nm and 18 nm, respectively. An electromagnetic pulse in the wavelength range from 400 to 800 nm was launched into a box containing the target NR in order to simulate a propagating plane wave to interact with the Au@Pt NR. The electromagnetic field was set to be polarized along the long axis of the Au@Pt NRs. The Au dielectric function determined by Palik [32] was used and the Au@Pt NRs were assumed to be embedded in water with a refractive index of 1.33.

3 Results and discussion

3.1 Gold nanorods (Au NRs)

A TEM image of the gold nanorods with a mean aspect ratio of 3.3 is shown in Fig. 1(a). Two plasmon absorption bands can be observed in case of gold nanorods corresponding to the oscillation of free electrons along and perpendicular to the long axis of the rods, called the longitudinal and transverse modes, respectively. The transverse mode is generally observed around 520 nm, and the longitudinal mode strongly depends on the aspect ratio, and is red-shifted with an increase in the aspect ratio of the nanorods [21]. The absorption spectrum of the Au NRs shown in Fig. 1(b) clearly indicates the presence of two absorption maxima at 511 and 738 nm corresponding to the transverse and longitudinal modes, respectively. A close inspection of the TEM image in Fig. 1(a) suggests that the particle shape can be approximated using a cylinder with rounded (semispherical) ends. The cylinder model is defined by the geometric parameters a and b, as shown in the inset of Fig. 2(a). FDTD results for a rod of $a = 38$ and $b = 16$ nm are given in Fig. 2. The extinction spectra are found to be in good agreement with the experimental spectra, as the transverse and longitudinal modes are observed at 518 and 740 nm, respectively.

Figures 2(c) and (d) represent the contours of the electromagnetic field enhancement $|E|^2$ of the transverse and longitudinal plasmon modes as a function of the angle, θ, between the rod axis and the polarization vector. The

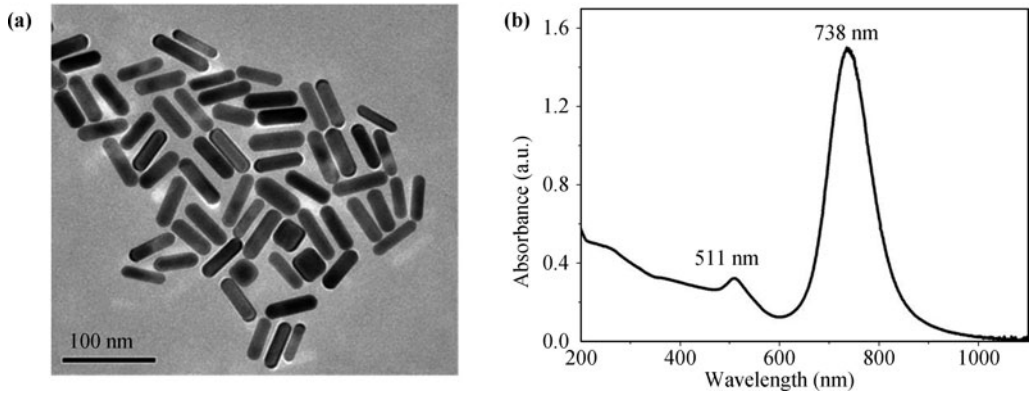

Fig. 1 **(a)** Typical TEM image and **(b)** UV-vis-NIR spectra of Au NRs.

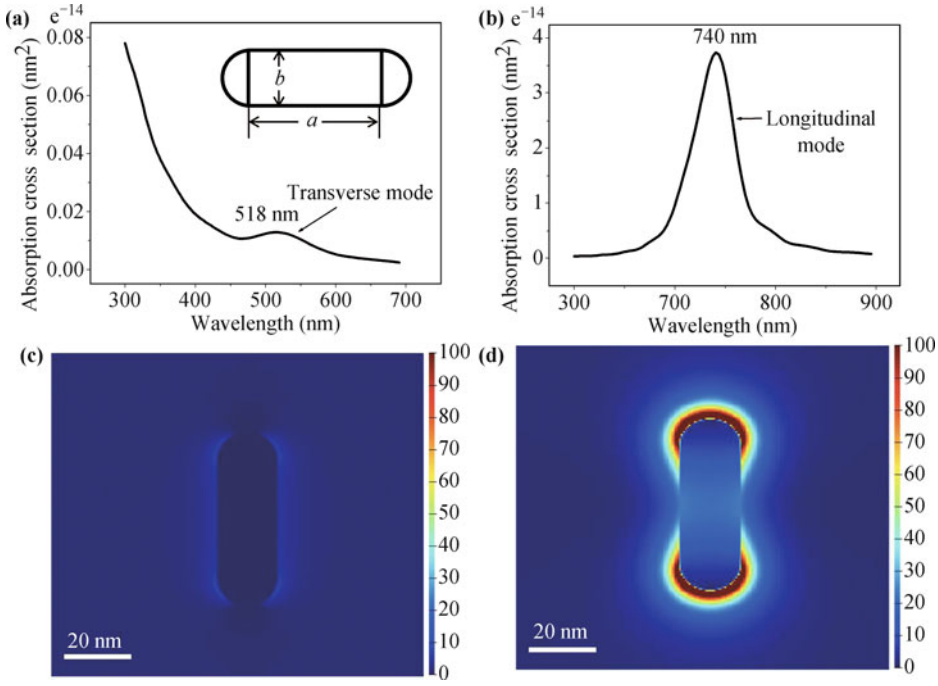

Fig. 2 Absorption cross section versus wavelength for **(a)** transverse and **(b)** longitudinal mode of gold nanorods. Electromagnetic field enhancement (contours of $|E|^2$) for **(c)** transverse and **(d)** longitudinal mode of gold nanorods.

values of $\theta = 90°$ and $\theta = 0°$ correspond to the transverse mode [Fig. 2(c)] and the longitudinal mode, respectively [Fig. 2(d)]. The transverse mode of the plasmon absorption of gold nanorods is found to be of less intensity compared to the longitudinal mode.

3.2 Au@Pt NRs

In order to apply the strategy of "borrowing", the most effective and feasible way is to coat the SERS-active substrate with a thin shell of transition metals [29]. Gold nanorods have been used as seeds for the platinum shell growth, and recent studies in the literature suggest that the growth of the platinum shells on gold nanorods occurs by two different mechanisms, resulting in nanodots coating or a smooth coverage of Pt on the gold nanorods [33, 34]. The strong electromagnetic field from the Au core is attenuated exponentially by an increase in the thickness of the Pt solid shell, however, is not completely shielded by the Pt nanodots [28]. To analyze this phenomenon theoretically, we used FDTD to estimate the electromagnetic field enhancement surrounding the core-shell nanoparticles.

In the case of solid shell growth mode, the enhanced electromagnetic field decays exponentially as the distance from the surface increases [Fig. 3(b)]. However, a substantially strong electromagnetic field enhancement can still be obtained in the case of Pt nanodots growth mode, even if the Pt nanodots are closely packed on the entire surface of the Au nanorods [Fig. 3(d)].

Our group has previously developed a procedure to grow Pt nanodots on gold nanorods [35] to form rod-shaped Au@Pt nanostructures with a Pt/Au ratio of 0.17 [Fig. 4(a)]. When the Pt nanodots are grown on the gold rods, a better homogeneity in the distribution of nanodots and a robust adhesion between the rod and the nanodots can be obtained.

TEM image and optical spectrum of the Au@Pt NRs are given in Fig. 4. Owing to the unique porous structure of the Pt nanodots, the transverse and longitudinal modes are red-shifted to 528 nm and 800 nm, respectively. The longitudinal SPR band undergoes a significant red-shift (100 nm) with a strong damping of intensity and a broadening of the width, as shown in Fig. 4(b).

The absorption spectra and the electromagnetic field enhancement contours obtained from the FDTD calculations are shown in Fig. 5. The thickness of the Pt shell is found to be 3 nm from the TEM measurements, indicating that the average diameter of the Pt nanodots is 3 nm. At lower Pt/Au ratios (Pt/Au ratios < 0.2), the Pt nanodots mainly appear at the end caps and side edges of the Au rod (Au nanorods have regular shape with 8 sharp corners and 8 edges [36]). Thus, the Pt nanodots

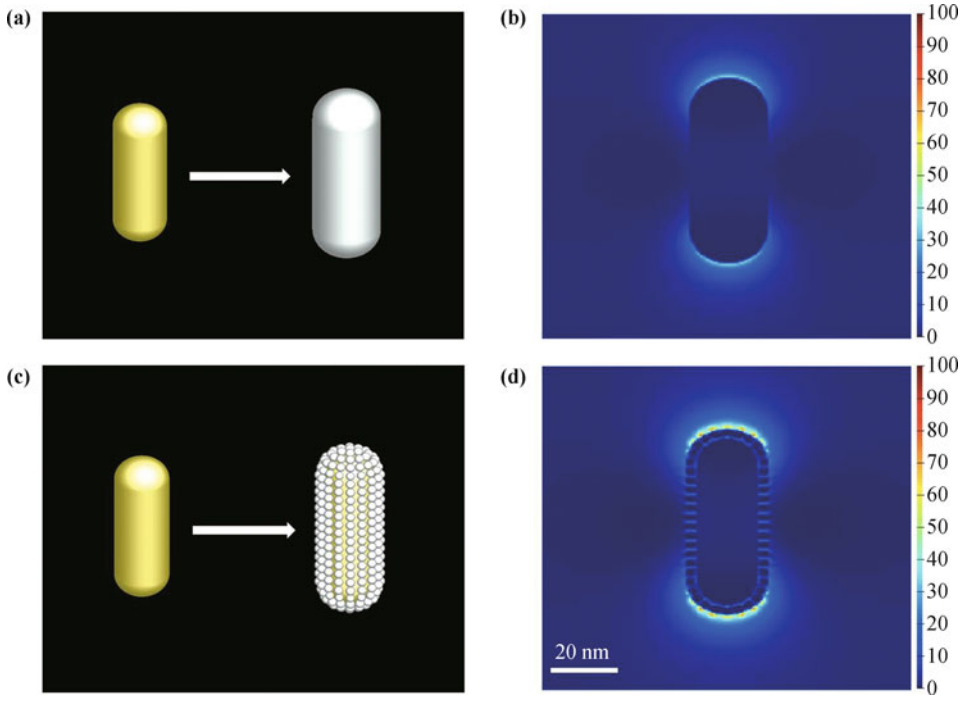

Fig. 3 The idealized 3D model of Au@Pt NR Au@Pt NRs with **(a)** Pt solid shell or **(c)** nanodots shell assumed for FDTD calculations and electromagnetic field enhancement (contours of $|E|^2$) for longitudinal mode of Au@Pt NR with **(b)** Pt solid shell or **(d)** nanodots shell. The thickness of the Pt solid shell is 3 nm and the Pt nanodots were assumed to be of spheres with a diameter of 3 nm.

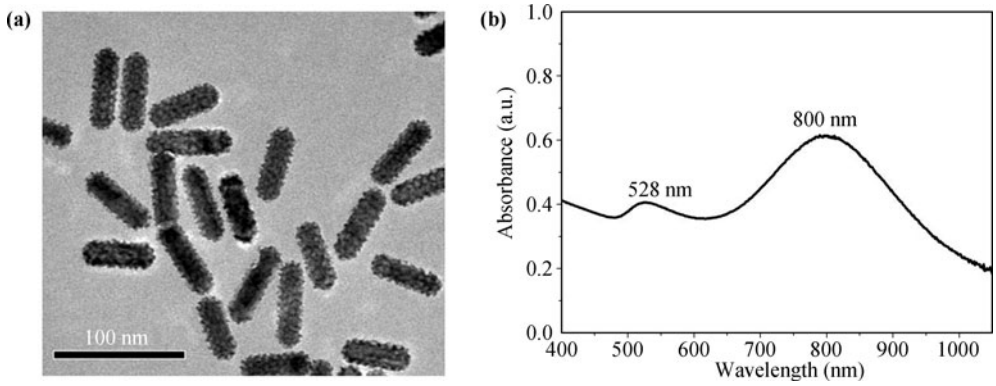

Fig. 4 **(a)** Typical TEM image and **(b)** UV-vis-NIR spectra of Au@Pt NRs.

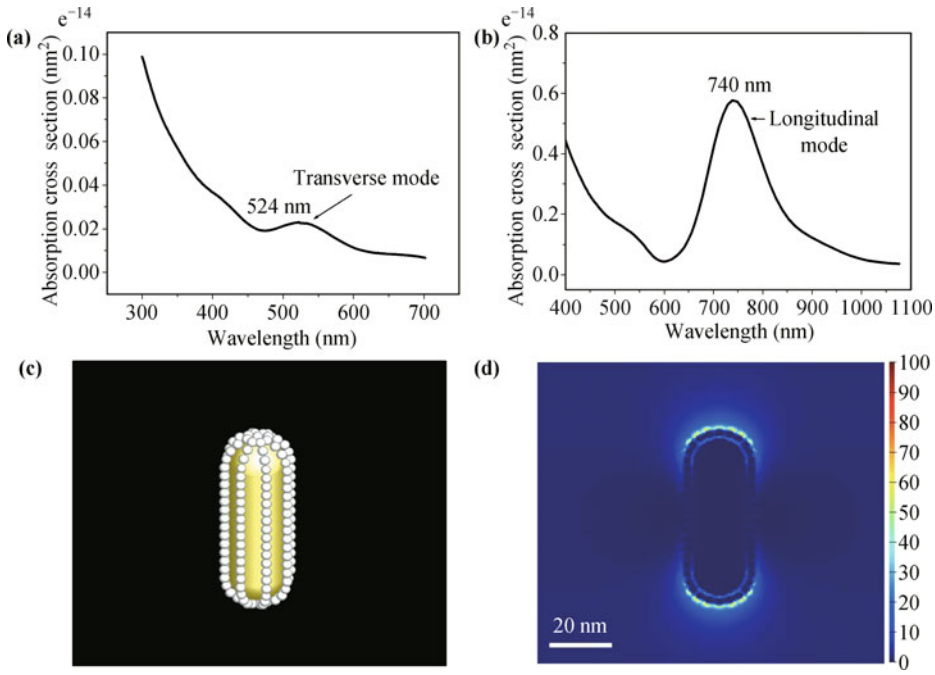

Fig. 5 Absorption cross section versus wavelength for **(a)** transverse and **(b)** longitudinal mode of Au@Pt NRs, **(c)** the idealized 3D model of Au@Pt NR assumed for FDTD calculations, and **(d)** electromagnetic field enhancement (contours of $|E|^2$) for longitudinal mode of Au@Pt NR. In this model of Au@Pt NR, Pt nanodots mainly appear at end caps and eight edges of the Au rods.

are assumed to be closely packed on the side-edges as shown in Fig. 5(c). In Fig. 5(b), a strong damping of the longitudinal SPR band is observed, but only a small shift in the resonance frequency is observed. This discrepancy between the calculated and measured values can be attributed to the changes in the nanorod shapes. Therefore, a detailed modeling is required to understand this behavior.

Considering the molar ratio of Pt/Au that was used in our experiments, the preferential edge-growth might not occur and the Pt dots may grow both at the edges and on the flat surfaces of the gold nanorods. As equal amounts of Pt were used, the number of Pt nanodots on every Au nanorod is considered the same for both Pt deposition modes. Thus, the Pt dots do not distribute closely at the entire Au NR surfaces [Fig. 6(a)].

The calculations show that this model can be used to explain the red shift in the plasmon resonances [Fig. 6(b)]. The longitudinal peak positions are in very good agreement with that in the experiments, but the resonance widths are consistently narrower in the simulations, as shown in Fig. 6(b). This might be due to performing calculations on a single nanorod, while in reality the samples contain particles with varying dimensions and Pt/Au ratios that result in the peak broadening. In comparison with Fig. 5(d), this geometric model provides a better enhancement of the electromagnetic field between the Pt nanodots.

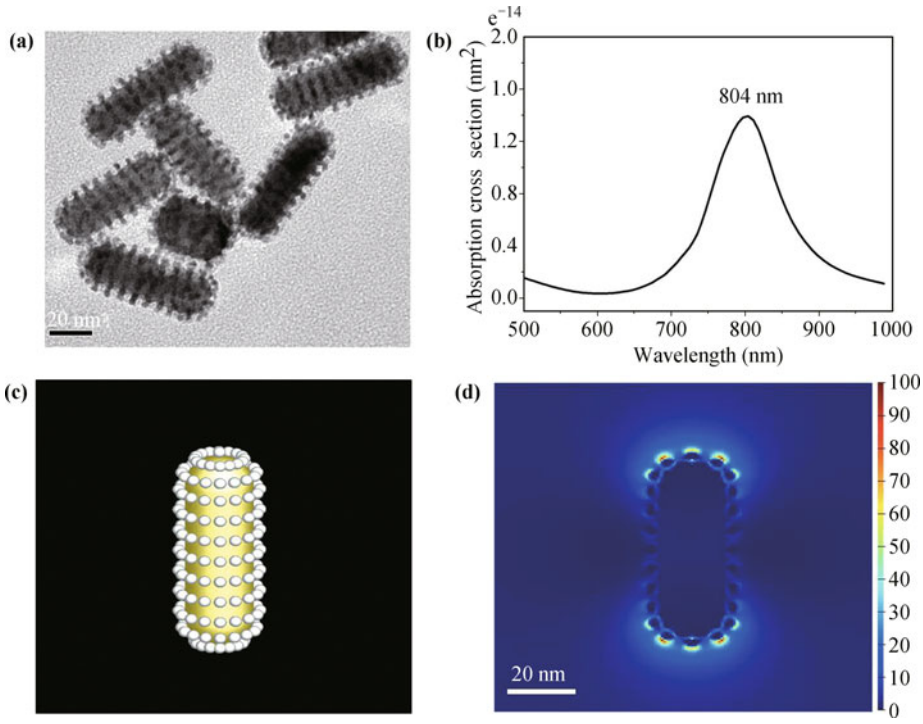

Fig. 6 **(a)** Typical TEM image of Au@Pt NRs, **(b)** absorption cross section versus wavelength for longitudinal mode of Au@Pt NRs, **(c)** the idealized 3D model of Au@Pt NR assumed for FDTD calculations, and **(d)** electromagnetic field enhancement (contours of $|E|^2$) for longitudinal mode of Au@Pt NR. In this model of Au@Pt NR, Pt dots form both at edges and on the flat surfaces of the Au rod.

Recent calculations consider a nano gap formed by several electromagnetically interacting particles generating a huge electromagnetic field. This near-field coupling effect is the origin of the "hot site" or "hot particle". Therefore, it would be of great interest to examine the morphology of the Pt nanodots deposited on the Au NRs to determine the effects of the Pt morphology on the electromagnetic field. Based on the SEM images of the samples, we suggest several geometrical morphologies for the calculations as below.

By finely tuning the growth conditions, the locations of the Pt nanodots can be tailored from end-caps to edges, and finally to the whole surface of the Au rod, as we have recently reported [35]. The morphology depends on the molar ratio of Pt/Au. Pt nanodots are preferentially formed at the edges at lower Pt/Au ratios and their density and distribution may be slightly different. In one case, Pt nanodots were formed only at four edges of the nanorods, leading to the formation of rectangular-shaped Au@Pt NRs [Fig. 7(a)]. In another case, small Pt nanodots were mainly observed on all the eight edges of the Au rod [Fig. 7(b)]. In accordance with the two different growth modes observed experimentally and based on the dimensions measured from the SEM images, we devised two geometrical morphologies for the calculations. As equal amounts of Pt were used, the number of Pt nanodots on every Au nanorod is considered the same for both Pt deposition modes. Thus, in the case of the four edges growth mode, Pt nanodots are closely packed on the edges [Fig. 7(c)]; and in the case of the eight edge growth mode, Pt nanodots are less closely packed [Fig. 7(d)].

Comparing the FDTD results of these two models, significant electromagnetic field enhancement between nanodots is obtained for the second system [Fig. 7(f)], i.e., the eight-edge growth mode. The low electromagnetic field enhancement observed for the first system [Fig. 7(e)], i.e., the four-edge growth mode. And the different results of these two growth modes need a specific discussion. When the nanodots are closely packed, it may be possible that the adjacent nanoparticles touch each other, closing the interparticle gap. These closed junctions cannot induce larger electromagnetic field enhancements, whereas in the other system the hot spots can be formed around the metal nanoparticles.

3.3 Au@Pt NRs with ends coating

Liz-Marzán's group has recently reported a preferential growth of Pt nanodots on the rod caps by manipulating the reduction conditions, where there was a high amount of silver ions [33]. In our experiment, we also obtained

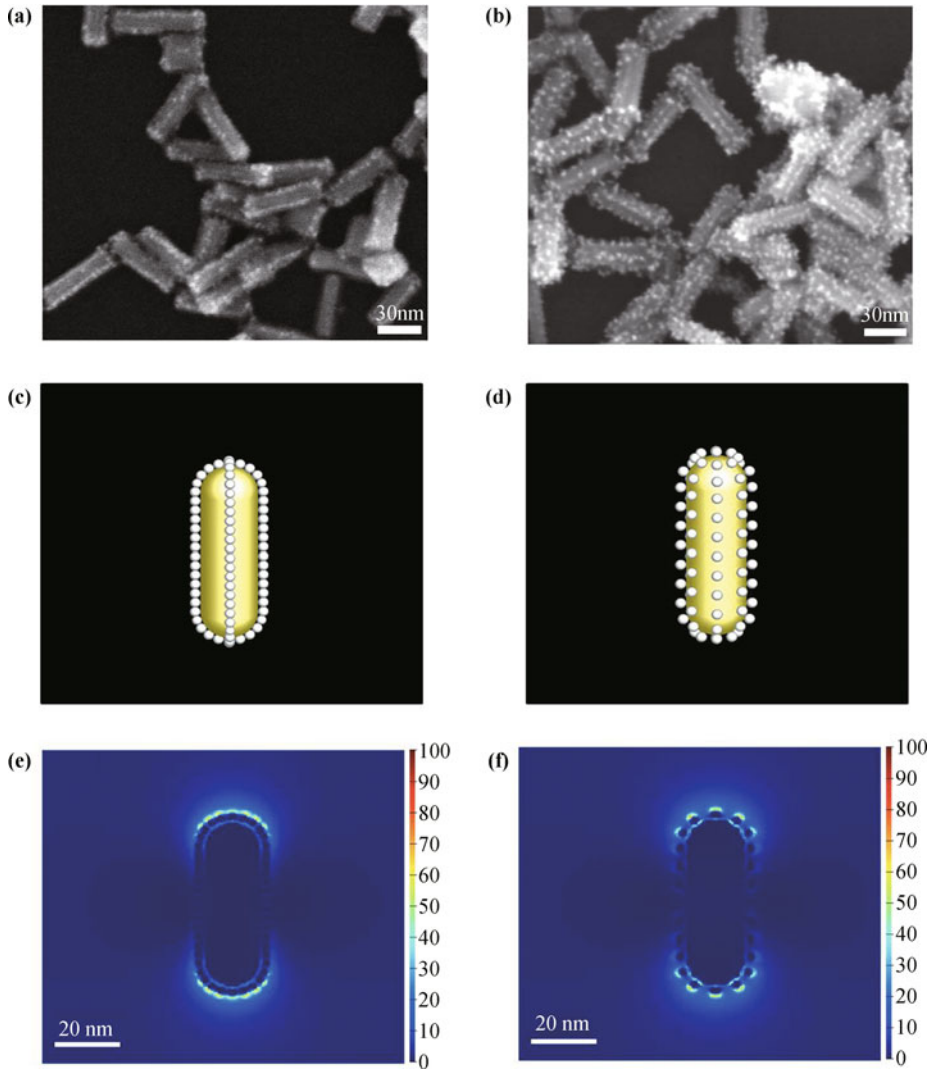

Fig. 7 **(a, b)** Typical SEM image of Au@Pt NRs; **(c, d)** the idealized 3D model of Au@Pt NRs assumed for FDTD calculations; **(e, f)** Electromagnetic field enhancement (contours of $|E|^2$) for longitudinal mode of Au@Pt NR. In the model of Au@Pt NR (a, c, e), Pt dots form at four edges of the Au rod and in the model of Au@Pt NR (b, d, f), Pt dots form at all eight edges of the Au rod.

Au@Pt NRs with end-coating. Pt nanodots are preferentially formed at the end caps with a Pt/Au ratio of 0.05 as can be seen in Fig. 8(a). Closely packed nanodots on the rod ends could also be obtained by a subsequent deposition of Pt on the precoated Pt dots [Fig. 8(b)]. "Hot spots" around the nanodots and a better electromagnetic field enhancement can be clearly observed in the case of less closely packed structures [Fig. 8(e)].

4 Conclusion

In summary, different morphologies of Au-core/Pt-shell nanorods have been analyzed by coating the Au-core with Pt or by depositing the nanodots at the end of the rods. We have investigated the optical property and electromagnetic field enhancement of Au@Pt NRs using the FDTD method, and the accuracy and validity of the FDTD calculations have been verified. The electromagnetic field enhancement is found to be rather independent of the Pt content, whereas the local roughness and small sharp features might significantly modify the near-field. As the electromagnetic field enhancement can be tuned by the distribution of Pt nanodots over the Au-core, Au@Pt NRs can find potential applications in related areas.

Acknowledgements This work was supported by the National Natural Science Foundation of China (Grant Nos. 11447200 and 21173056), the Natural Science Foundation of Shandong Province of China (Grant No. ZR2014BP014), the Key Research and Development Program of Shandong Province of China (Grant No. 2015GSF118079), the Project of Science and Technology

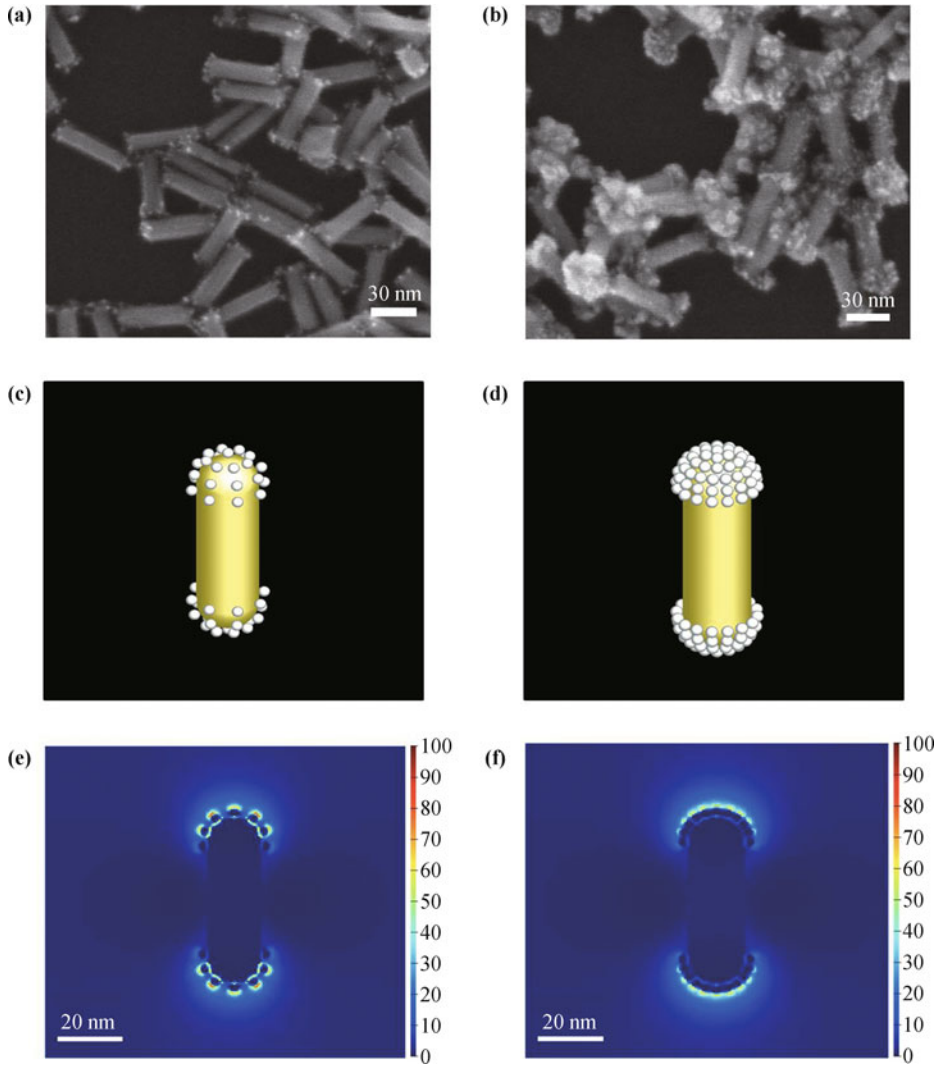

Fig. 8 **(a, b)** Typical SEM images of Au@Pt NR; **(c, d)** the idealized 3D model of Au@Pt NR assumed for FDTD calculations; **(e, f)** Electromagnetic field enhancement (contours of $|E|^2$) for longitudinal mode of Au@Pt Ns. In the model of Au@Pt NR (a, c, e) non-close-packed Pt dots on end caps of the Au rod and in the model of Au@Pt NR (b, d, f), close-packed Pt dots on end caps of the Au rod.

Development Program in Shandong Province of China (Grant Nos. 2011YD01101, 2013YD2008, and 2013YD02054), and the Project of Shandong Province Higher Educational Science and Technology Program (Grant No. J13LN08).

References

1. X. H. Xia and Y. N. Xia, Gold nanocages as multifunctional materials for nanomedicine, *Front. Phys.* 9(3), 378 (2014)
2. S. Linic, P. Christopher, H. Xin, and A. Marimuthu, Catalytic and photocatalytic transformations on metal nanoparticles with targeted geometric and plasmonic properties, *Acc. Chem. Res.* 46(8), 1890 (2013)
3. R. Ghosh Chaudhuri, and S. Paria, Core/shell nanoparticles: Classes, properties, synthesis mechanisms, characterization, and applications, *Chem. Rev.* 112(4), 2373 (2012)
4. O. Nicoletti, F. de La Peña, R. K. Leary, D. J. Holland, C. Ducati, and P. A. Midgley, Three-dimensional imaging of localized surface plasmon resonances of metal nanoparticles, *Nature* 502(7469), 80 (2013)
5. Y. L. Zhao, Y. L. Song, W. G. Song, W. Liang, X. Y. Jiang, Z. Y. Tang, H. X. Xu, Z. X. Wei, Y. Q. Liu, M. H. Liu, L. Jiang, X. H. Bao, L. J. Wan, and C. L. Bai, Progress of nanoscience in China, *Front. Phys.* 9(3), 257 (2014)
6. Z. Y. Li, Nanophotonics in China: Overviews and highlights, *Front. Phys.* 7(6), 601 (2012)
7. J. S. Miao, W. D. Hu, Y. L. Jing, W. J. Luo, L. Liao, A. L. Pan, S. W. Wu, J. X. Cheng, X. S. Chen, and W. Lu, Surface plasmon-enhanced photodetection in few layer MoS_2 phototransistors with Au nanostructure arrays, *Small* 11(20), 2392 (2015)
8. S. P. Zhang, H. Wei, K. Bao, U. Hakanson, N. J. Halas, P. Nordlander, and H. X. Xu, Chiral surface plasmon polari-

tons on metallic nanowires, *Phys. Rev. Lett.* 107(9), 096801 (2011)

9. S. J. Barrow, X. Wei, J. S. Baldauf, A. M. Funston, and P. Mulvaney, The surface plasmon modes of self-assembled gold nanocrystals, *Nat. Commun.* 3, 1275 (2012)
10. L. M. Tong and H. X. Xu, Frontiers of plasmonics, *Front. Phys.* 9(1), 1 (2014)
11. R. A. Alvarez-Puebla, A. Agarwal, P. Manna, B. P. Khanal, P. Aldeanueva-Potel, E. Carbó-Argibay, N. Pazos-Pérez, L. Vigderman, E. R. Zubarev, N. A. Kotov, and L. M. Liz-Marzan, Gold nanorods 3D-supercrystals as surface enhanced Raman scattering spectroscopy substrates for the rapid detection of scrambled prions, *Proc. Natl. Acad. Sci. USA* 108(20), 8157 (2011)
12. E. C. Le Ru and P. G. Etchegoin, Single-molecule surface-enhanced Raman spectroscopy, *Annu. Rev. Phys. Chem.* 63(1), 65 (2012)
13. G. McNay, D. Eustace, W. E. Smith, K. Faulds, and D. Graham, Surface-enhanced raman scattering (SERS) and surface-enhanced resonance Raman scattering (SERRS): A review of applications, *Appl. Spectrosc.* 65(8), 825 (2011)
14. Y. S. Yamamoto, M. Ishikawa, Y. Ozaki, and T. Itoh, Fundamental studies on enhancement and blinking mechanism of surface-enhanced Raman scattering (SERS) and basic applications of SERS biological sensing, *Front. Phys.* 9(1), 31 (2014)
15. Z. Kim, Single-molecule surface-enhanced Raman scattering: Current status and future perspective, *Front. Phys.* 9(1), 25 (2014)
16. Y. Zhang, J. Qian, D. Wang, Y. L. Wang, and S. L. He, Multifunctional gold nanorods with ultrahigh stability and tunability for in vivo fluorescence imaging, SERS detection, and photodynamic therapy, *Angew. Chem. Int. Ed.* 52(4), 1148 (2013)
17. N. A. Hatab, C. H. Hsueh, A. L. Gaddis, S. T. Retterer, J. H. Li, G. Eres, Z. Zhang, and B. Gu, Free-standing optical gold bowtie nanoantenna with variable gap size for enhanced raman spectroscopy, *Nano Lett.* 10(12), 4952 (2010)
18. K. H. Su, S. Durant, J. M. Steele, Y. Xiong, C. Sun, and X. Zhang, Raman enhancement factor of a single tunable nanoplasmonic resonator, *J. Phys. Chem. B* 110(9), 3964 (2006)
19. L. J. Sherry, R. Jin, C. A. Mirkin, G. C. Schatz, and R. P. Van Duyne, Localized surface plasmon resonance spectroscopy of single silver triangular nanoprisms, *Nano Lett.* 6(9), 2060 (2006)
20. S. Wang, D. F. Pile, C. Sun, and X. Zhang, Nanopin plasmonic resonator array and its optical properties, *Nano Lett.* 7(4), 1076 (2007)
21. Y. Z. He, J. X. Fu, and Y. P. Zhao, Oblique angle deposition and its applications in plasmonics, *Front. Phys.* 9(1), 47 (2014)
22. F. Z. Cong, H. Wei, X. R. Tian, and H. X. Xu, A facile synthesis of branched silver nanowire structures and its applications in surface-enhanced Raman scattering, *Front. Phys.* 7(5), 521 (2012)
23. W. Y. Rao, Q. Li, Y. Z. Wang, T. Li, and L. J. Wu, Comparison of photoluminescence quantum yield of single gold nanobipyramids and gold nanorods, *ACS Nano* 9(3), 2783 (2015)
24. S. Khatua, P. M. Paulo, H. Yuan, A. Gupta, P. Zijlstra, and M. Orrit, Resonant plasmonic enhancement of single-molecule fluorescence by individual gold nanorods, *ACS Nano* 8(5), 4440 (2014)
25. Z. L. Zhang, L. Chen, S. X. Sheng, M. T. Sun, H. R. Zheng, K. Q. Chen, and H. X. Xu, High-vacuum tip enhanced Raman spectroscopy, *Front. Phys.* 9(1), 17 (2014)
26. B. Sharma, R. R. Frontiera, A. I. Henry, E. Ringe, and R. P. Van Duyne, SERS: Materials, applications, and the future, *Mater. Today* 15(1–2), 16 (2012)
27. K. Ikeda, J. Sato, N. Fujimoto, N. Hayazawa, S. Kawata, and K. Uosaki, Plasmonic enhancement of Raman scattering on non-SERS-active platinum substrates, *J. Phys. Chem. C* 113(27), 11816 (2009)
28. J. F. Li, Z. L. Yang, B. Ren, G. K. Liu, P. P. Fang, Y. X. Jiang, D. Y. Wu, and Z. Q. Tian, Surface-enhanced Raman spectroscopy using gold-core platinum-shell nanoparticle film electrodes: toward a versatile vibrational strategy for electrochemical interfaces, *Langmuir* 22(25), 10372 (2006)
29. Z. Q. Tian, B. Ren, J. F. Li, and Z. L. Yang, Expanding generality of surface-enhanced Raman spectroscopy with borrowing SERS activity strategy, *Chem. Commun.* (34), 3514 (2007)
30. L. P. Xia, Z. Yang, S. Y. Yin, W. R. Guo, J. L. Du, and C. L. Du, Hole arrayed metal-insulator-metal structure for surface enhanced Raman scattering by self-assembling polystyrene spheres, *Front. Phys.* 9(1), 64 (2014)
31. N. R. Jana, L. Gearheart, and C. J. Murphy, Seed-mediated growth approach for shape-controlled synthesis of spheroidal and rod-like gold nanoparticles using a surfactant template, *Adv. Mater.* 13(18), 1389 (2001)
32. D. W. Lynch and W. R. Hunter, in: Handbook of Optical Constants of Solids, edited by E. D. Palik, New York: Academic Press, 1985, pp 350–356
33. M. Grzelczak, J. Pérez-Juste, B. Rodríguez-González, and L. M. Liz-Marzán, Influence of silver ions on the growth mode of platinum on gold nanorods, *J. Mater. Chem.* 16(40), 3946 (2006)
34. M. Grzelczak, J. Perez-Juste, F. J. García de Abajo, and L. M. Liz-Marzán, Optical properties of platinum-coated gold nanorods, *J. Phys. Chem. C* 111(17), 6183 (2007)
35. L. L. Feng, X. C. Wu, L. R. Ren, Y. J. Xiang, W. W. He, K. Zhang, W. Y. Zhou, and S. S. Xie, Well-controlled synthesis of Au@Pt nanostructures by gold-nanorod-seeded growth, *Chem. Eur. J.* 14(31), 9764 (2008)
36. Z. L. Wang, M. Mohamed, S. Link, and M. El-Sayed, Crystallographic facets and shapes of gold nanorods of different aspect ratios, *Surf. Sci.* 440(1–2), L809 (1999)